Analysis of Piezoelectric Structures and Devices

Analysis of Piezoelectric Structures and Devices

Edited by
Daining Fang
Ji Wang
Weiqiu Chen

De Gruyter 高等教育出版社 HIGHER EDUCATION PRESS

Physics and Astronomy Classification Scheme 2010: 77.65.-j, 85.50.-n, 77.84.-s, 77.65.Dq, 77.84.Lf

ISBN 978-3-11-029788-1
e-ISBN 978-3-11-029799-7

Library of Congress Cataloging-in-Publication Data

A CIP catalog record for this book has been applied for at the Library of Congress.

Bibliographic information published by the Deutsche Nationalbibliothek

The Deutsche Nationalbibliothek lists this publication in the Deutsche Nationalbibliografie; detailed bibliographic data are available in the Internet at http://dnb.dnb.de.

Printing and binding: Hubert & Co. GmbH & Co. KG, Göttingen
♾ Printed on acid-free paper

Printed in Germany

www.degruyter.com

Preface

Typical piezoelectric structures of devices such as resonators, actuators, and transducers have been known as targets for analysis with the consideration of coupled fields including mechanical, electrical, and thermal, to name a few, in applications concerning electronic functions for frequency control and detection and sensors for data collection. Indeed, utilization of piezoelectric structures with primary objective of accurate vibration frequency has been found in a wide arrange of practical problems and in-depth studies are required particularly in the strongly demanded biological and chemical sensor technology as sensing elements. To meet application needs, research work focusing on issues in the analysis of piezoelectric elements in devices and structures for sensor and control applications has been conducted for refined predictions of characteristics and behavior towards optimal design and improvement. Such methods and solutions are widely presented in conferences and publications of applied mechanics, which is not well communicated with application engineers of electronic devices for many reasons.

The core requirements for the analysis of piezoelectric structures are deformation, vibration frequency, mode shapes, electric potential, and electric charge distribution, among others. These results can be used for the precise design of device structures for sensor and actuator applications with properties in terms of both mechanical and electrical variables. It is clear that the precise analysis is the key to good design which can be better achieved with analytical techniques rather than empirical approaches through the combination of experiments and experiences of good and acceptable designs. To this goal, many works have been done with analytical solutions based on approximate theories with the consideration of configuration, materials, and complications. Such theories have also been expanded to consider the coupled fields required in the analysis of devices with primary considerations of thermal and electrical variables, which are also needed in the formulation and estimation of electrical parameters. Indeed, such efforts have been successful in certain applications with sophisticated methods and techniques for the analysis and design of devices and structures meeting the precision needs of product development such as quartz crystal resonators based on the Mindlin plate equations and follow-up expansion for the thermal considerations. In addition, the Mindlin plate equations have been extended to the finite element analysis for accurate and practical analysis. The advantage of approximate theory has been well demonstrated with the accuracy and simplicity of such analysis with both analytical techniques and numerical methods, showing benefits of approximate methods as one of the needed proofs for further research on the methods. It is certainly well accepted in device and structure analysis because similar efforts have been made in related manners and the results in accelerated analysis have been embraced through improvements.

To summarize recent progress on the analysis of piezoelectric structures in engineering applications, we have invited a few active researchers on this subject matter to provide state-of-art accounts on a few topics with broad interests. From these contributions, we can find original research work closely related to structural analysis, device design, fundamental theory, complication factors, and performance evaluation through both theoretical and experimental approaches. Such theory and methods are important in many applications such as actuators, energy harvesters, sensors, resonators with the consideration of novel materials (photostrictive, multiferroic, functionally graded, layered) and various configurations (plates, shells, composites). The wave modes involved in the analysis cover the commonly utilized surface acoustic waves (SAW), bulk acoustic waves (BAW) as the key functioning modes for extensive studies. In addition, there are novel approaches to establish new methods and techniques for the analysis of traditional device structures for possible fast and accurate predictions of essential vibration properties such as the frequency, mode shapes, charge distribution, and effects of complication factors such as surface, thermal, acceleration, stress, electric field and drive-level, and so on. These results can be used not only for the validation and optimization of designs, but also in the calculation of electrical parameters of devices which are commonly functioning as electrical elements in modern electronic circuits. The importance of such analytical techniques and methods is increasingly apparent not only in the computer-based product development process with advantages over time and cost but also international collaboration in the manufacturing and product conceiving process. Clearly, major efforts pioneered through such research should be appreciated and further advances with emphasis on the experimental validation of analytical models and results to improve the product development cycle without any gap left should also be encouraged.

The overall research on the acoustic wave devices and structures involving materials, physical acoustics, and electrical parameters has been active in core groups meeting the growing need of new types of electronic and intelligent products, and many of the contributors of this volume have been playing leading roles in research and teaching. More importantly, these active researchers are also heading different directions in diversified communities and groups spanning geologically in the electronic, materials, physical acoustic, and mechanics fields. Such activities will bring the urgent technical challenges to be known by more engineers and scientists with the expected outcome of enriched know ledge and increased involvement in research and studying. Undoubtedly, this will make the subject matters more appealing to generations of students and practical engineers as we have been hoping. This book present the frontiers of piezoelectric structures and devices research in a unified and grouped collection, and will certainly help students, engineers, professors, and technologists to find the information and methods needed to guide their participation and anticipation in the field and industry. This is the latest addition to our dedication of a broader professional and technical exchange through conferences such as the IEEE Frequency Control and Ultrasonics Symposia, the SPAWDA, and other workshops and meetings we have been organizing in last decades.

Editors

Daining Fang	Ji Wang	Weiqiu Chen
Peking University	Ningbo University	Zhejiang University

August, 2012

Contents

Chapter 1

Non-uniform Actuations of Plates and Shells with Piezoelectric and Photostrictive Skew-quad Actuator Designs

Jing Jiang[1], HongHao Yue[1], ZongQuan Deng[1], and HornSen Tzou[2]
[1]*School of Mechatronic Engineering, Harbin Institute of Technology, Harbin, 150001, China*
[2]*Institute of Applied Mechanics, StrucTronics and Control Lab., School of Aeronautics and Astronautics, Zhejiang University, Hangzhou, 310027, China*

Abstract Conventional distributed actuators laminated on shells and plates usually only introduce uniform control forces and moments. Structural actuation and control based on uniform control forces and moments have been investigated for over two decades. This study is to exploit a new actuator design, i.e., a skew-quad (SQ) actuator system made of piezoelectric and photostrictive materials. This new actuator system composed of four regions can induce non-uniform control forces and moments owing to the uneven boundary conditions of each region. The non-uniform distribution of actuator induced forces and moments are defined based on the variation method and validated by ANSYS. The coupling equation of a simply supported plate laminated with the piezoelectric SQ actuator is derived. Distributed control action resulting from the non-uniform control moments is also defined in the modal domain. Control actions of center-placed and corner-placed actuators on a square plate are defined and compared. Furthermore, wireless non-contact actuation of cylindrical shells coupled with the center-placed and corner-placed photostrictive SQ actuator systems are evaluated respectively. The modal control actions change with respect to the modes and the actuator coverage and thus, the actuator size and location are very important to the modal control effectiveness. In order to improve the control actions of the SQ actuator system, control schemes are designed for piezoelectric and photostrictive SQ actuator system respectively to regulate the sign of control forces of each region and to improve actuation effectiveness.
Keywords distributed control, plate, cylindrical shell, piezoelectric and photostrictive actuator design, non-uniform control action

1.1 Introduction

Spatially distributed vibration control of flexible structures with distributed actuators has been extensively studied for over two decades [1-5]. Earlier studies indicate that actuator design and placements are crucial to effective actuation and control of distributed parameter systems (DPSs), e.g., shells and plates [6-11]. A number of different design configurations, e.g., segmentation [12-16] and shaping [17-20], have been thoroughly evaluated over the years. Most of these actuator designs usually induce uniform control forces and moments. The inherent uniformly distributed control forces and control moments, however, often limit the control effectiveness and efficacy of structures. For example, a single-piece centrally and symmetrically placed distributed actuator reveals control deficiencies to anti-symmetrical modes of symmetrical structures [12,13]. This symmetry problem can be resolved by spatially regulating the output characteristics of actuators [2,21], which can be realized by spatially varying either control signals or thickness of actuators. Sullivan et al. [2] proposed an approximation to a continuous non-uniform distribution of control actions with a combination of gain-weighted and shaped transducers. In this study, a new actuator design, with the two inner adjacent edges fixed and the other two edges freed, is proposed and evaluated. The actuator's boundary conditions are specifically selected to realize the continuous non-uniform distribution of actuator induced control forces and control moments. Based on the variation method [22], the non-uniform distribution functions of induced forces and moments are calculated and validated. A new skew-quad (SQ) actuator design composed of four regions of the above actuator configuration is proposed and its actuation effectiveness to flexible structures is evaluated. Due to the novel design and the boundary conditions of its each region, this new SQ actuator system can induce multi-DOF (degree-of-freedom) non-uniform control forces and moments and consequently lead to stronger control actions at its four corners. New SQ actuator systems composed of piezoelectric and photostrictive actuation mechanisms are respectively discussed next. Control actions of piezoelectric and photostrictive SQ actuator systems with different surface coverage, location and control scheme are respectively evaluated in case studies.

Piezoelectric actuation is based on the converse piezoelectric effect. Distributed actuation and control of shells and plates or DPSs have been investigated [21]. Among commonly used piezoelectric materials, flexible polymeric polyvinylidene fluoride (PVDF) film is versatile in shell applications, owing to its flexibility, durability, sensitivity, manufacturability, etc. [23]. The coupling equations of a simply supported plate laminated with the piezoelectric SQ actuator system is derived based on the generic distributed sensing and control theories of thin shells [21,24,25]. Distributed control action is also defined in the modal domain. Control effects of two locations, i.e., center-located and corner-located, of the new SQ actuator are evaluated respectively. In each case, control actions with different surface coverage (i.e., actuator sizes) are evaluated in the first part of this chapter. Furthermore, in order to reduce control deficiencies on anti-symmetrical modes of symmetrical plates when the new SQ actuator is centrally and symmetrically placed, four segmented sensors are also used to regulate the sign of control voltages in each region and their control effectiveness is also evaluated. Photostrictive actuation of shells is discussed next and detailed actuation characteristics of shells are presented in the second part of the chapter.

Conventional actuators, e.g., piezoelectric, require hard-wire connections to transmit energy sources and control commands to activate the actuator mechanisms. The hard-wire signal transmission busses can easily attract undesirable electric noises influenced by electric and/or magnetic fields. Accordingly, noises and uncertainties are often involved and control commands may not be accurately executed. Opto-mechanical actuators controlled by high-energy lights represent a new class of non-contact precision actuators based on the photodeformation process [26]. Irradiating high-energy lights, such as lasers or ultraviolet lights, on a certain class of photostrictive materials can trigger the photodeformation and, consequently, the induced photodeformation can be used for non-contact precision actuation and control. Light-driven opto-mechanical actuators have many advantages over conventional hard-wired electromechanical actuators, such as ① high electrical output voltage, ② non-contact actuation, ③ compact and lightweight, ④ immune from electric/magnetic disturbances, and ⑤ remote control. One-dimensional (beam type) and two-dimensional (plate type) opto-mechanical actuators with applications to distributed vibration control have been investigated [27-31]. Multi-DOF photostrictive actuators are proposed and their performance are evaluated [32,33]. In the second part of this chapter, cylindrical shell control with the photostrictive SQ actuator system made of four single-piece photostrictive slabs is investigated. Uniform and non-uniform micro-photodeformations are defined first. Photostrictive SQ actuator system design and its non-uniform actuation behavior are discussed, followed by modal control effectiveness of a flexible cylindrical panel respectively coupled with the center-placed and corner-placed new SQ actuator systems. Closed-loop actuation to improve control effectiveness of unsymmetrical shell modes is also evaluated. Again, distributed control actions of piezoelectric and photostrictive SQ actuator systems with different surface coverage, location and control scheme are respectively reported in this chapter.

1.2 New SQ actuator system

As discussed previously, uniform actuation and control of shells and plates have been studied over the years. Non-uniform actuation and control are emphasized in this chapter. An actuator element with uneven boundary conditions is introduced first and its non-uniform actuation behavior is evaluated. A new SQ actuator design based on the actuator element is proposed and its actuation effectiveness to plates and shells are presented later.

1.2.1 The distribution profile of induced non-uniform forces and moments

When a control voltage is applied to an unconstrained piezoelectric actuator, the actuator usually induces uniform strains or actuations. However, an actuator can induce non-uniform strains when its boundary conditions are carefully manipulated. As shown in Fig.1.1, an actuator element, with the two inner adjacent edges fixed and the other two edges freed, can induce non-uniform strains or actuations. In this section, the non-uniform deformation and actuation behavior is evaluated.

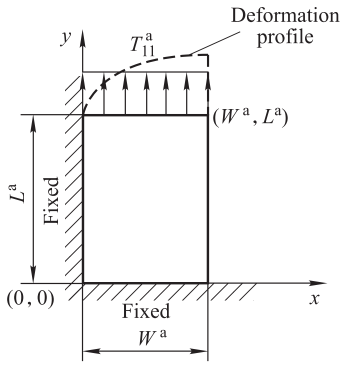

Fig. 1.1 An actuator element with fixed-fixed-free-free boundary conditions.

When a control voltage is applied to a single mono-axial piezoelectric piece fixed at one end, the actuator element induces a uniform strain

$$\overline{S} = \frac{d_{31}\phi^{a}}{h^{a}} \tag{1.1}$$

where d_{31} is the piezoelectric constant, ϕ^{a} is a control voltage applied to the actuator, and h^{a} is the actuator thickness. The equivalent uniform tension stress T_{11}^{a} exerted by the actuator can be expressed as

$$T_{11}^{a} = \frac{d_{31}Y_{a}\phi^{a}}{h^{a}} = \overline{S}Y_{a} \tag{1.2}$$

where Y_{a} is Young's modulus of the piezoelectric actuator. However, with the boundary conditions shown in Fig.1.1, the deformation is obviously zero at the fixed side and the deformation is the maximum at the free corner. This deformation profile (or an equivalent force profile when fixed) can be calculated using the variation method. Because of the linear relationship between the actuator deformation and the tension stress T_{11}^{a}, the magnitude of T_{11}^{a} is normalized, i.e., 1, to simplify the profile calculation. Thus, the true deformation is the calculated value multiplied by the true actuator stress T_{11}^{a}, once the actuator material, control signal and dimensions are specified. Since the actuator is very thin, this is a plane problem in elasticity. According to the displacement boundary conditions, this problem can be solved by the planar displacement variation method. The displacements in the x and y directions can be respectively set as

$$u = u_0 + \sum_m A_m u_m \tag{1.3}$$

$$v = v_0 + \sum_m B_m v_m \tag{1.4}$$

where u and v are the displacements in the x and y directions respectively; A_m and B_m are $2m$ independent coefficients; and u_0, v_0, u_m and v_m are functions set to satisfy the given boundary conditions. The boundary values of u_0 and v_0 are equal to the known boundary displacements; the values of u_m and v_m are zero on this boundary in this case. The boundary conditions is illustrated in Fig.1.1, i.e., $u(x,y)(x=0,y=0)=0$, $v(x,y)(x=0,y=0)=0$, and hence $u_0=0$, $v_0=0$. The x and y displacement functions are assumed to be

$$\begin{aligned} u(x,y) &= xy(A_1 + A_2 y + A_3 xy + A_4 x + A_5 xy^2 + A_6 x^2 y + A_7 x^2 y^2 + A_8 x^2 y^3 \\ &\quad + A_9 x^3 y^2 + A_{10} x^3 y^3 + A_{11} x^3 y^4 + \cdots) \qquad (1.5) \\ v(x,y) &= xy(B_1 + B_2 x + B_3 xy + B_4 y + B_5 x^2 y + B_6 xy^2 + B_7 x^2 y^2 + B_8 x^3 y^2 \\ &\quad + B_9 x^2 y^3 + B_{10} x^3 y^3 + B_{11} x^4 y^3 + \cdots) \qquad (1.6) \end{aligned}$$

The potential energy for a plane stress problem can be expressed as [22]

$$V_\varepsilon = \frac{Y_\mathrm{a}}{2(1-\mu^2)} \iint \left[\left(\frac{\partial u}{\partial x}\right)^2 + \left(\frac{\partial v}{\partial y}\right)^2 + 2\mu \frac{\partial u}{\partial x}\frac{\partial v}{\partial y} + \frac{(1-\mu)}{2}\left(\frac{\partial v}{\partial x} + \frac{\partial u}{\partial y}\right)^2 \right] \mathrm{d}x\mathrm{d}y \tag{1.7}$$

where V_ε is the deformation potential energy, μ is actuator's Poisson's ratio. The $2m$ coefficients can be derived by

$$\frac{\partial V_\varepsilon}{\partial A_m} = \iint f_x u_m \mathrm{d}x\mathrm{d}y + \int \overline{f_x} u_m \mathrm{d}s \tag{1.8}$$

$$\frac{\partial V_\varepsilon}{\partial B_m} = \iint f_y v_m \mathrm{d}x\mathrm{d}y + \int \overline{f_y} v_m \mathrm{d}s \tag{1.9}$$

where f_x and f_y are body forces, $\overline{f_x}$ and $\overline{f_y}$ are surface forces acted on the actuator respectively in the x and y directions. As shown in Fig.1.1, the body forces $f_x = f_y = 0$ and the surface forces $\overline{f_y} = T_{11}^\mathrm{a}$, $\overline{f_x} = 0$. The $2m$ independent coefficient A_m and B_m can be determined by solving Eqs.(1.5)-(1.9). The calculated displacement changes with respect to the number of coefficients m. The parameters of this single-piece actuator element are $L^\mathrm{a} = 0.05$ m, $W^\mathrm{a} = 0.05$ m, $Y_\mathrm{a} = 2.0 \times 10^9$ N/m^2. The induced deformation in the y direction of the corner point $(W^\mathrm{a}, L^\mathrm{a})$ with respect to coefficients m are summarized in Table 1.1. Analysis results indicate that when the number of coefficients m is set to 6, 7, 8, 9 and 10, solutions of the corner displacement is consistent with each other, i.e., the displacement solution is converged. In later calculations, the number of coefficients is set as 10.

Table 1.1 Solutions obtained by the variation method.

Number of coefficients	6	7	8	9	10
Corner displacement /($\times 10^{-11}$m)	2.638	2.661	2.635	2.634	2.637

In order to validate the results, the actuator deformation profile is also calculated by the finite element software ANSYS. The two displacement curves calculated respectively by ANSYS and by the variation method are plotted in Fig.1.2 and they do compare very favorably. Thus, the deformation profile of one mono-axial actuator element with the boundary condition of two inner adjacent edges fixed and the other two edges freed is defined and the actuation force can also be derived accordingly.

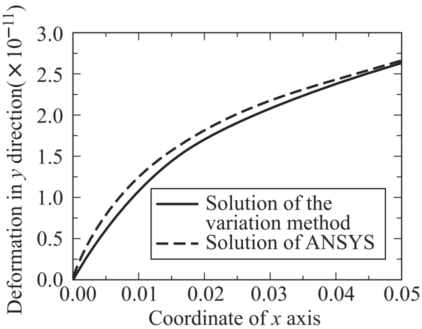

Fig. 1.2 Comparison of actuator deformations.

When m is set to 10, the actuator deformation in the y direction shown in Fig.1.2 can be expressed as

$$\begin{aligned} v(x,y) = xy(&B_1 + B_2x + B_3xy + B_4y + B_5x^2y + B_6xy^2 \\ &+ B_7x^2y^2 + B_8x^3y^2 + B_9x^2y^3 + B_{10}x^3y^3) \end{aligned} \tag{1.10}$$

The total actuator deformation in the y direction can be defined by substituting $y = L^{\mathrm{a}}$ into Eq.(1.10). Thus, the induced equivalent actuator strain can be written as

$$\overline{S}' = \frac{T_{11}^{\mathrm{a}} v(x, L^{\mathrm{a}})}{L^{\mathrm{a}}} = \frac{\overline{S} Y_{\mathrm{a}} v(x, L^{\mathrm{a}})}{L^{\mathrm{a}}} \tag{1.11}$$

The non-uniform actuation force of the actuator element can be defined accordingly. Design of a new SQ actuator system and its control forces and moments are discussed next.

1.2.2 Design of an SQ actuator system

A new SQ actuator system is made of four regions (Fig.1.3). Two inner adjacent edges of each region of the SQ system are fixed to a stable cross fixture and the other two outer adjacent edges are free. With these boundary conditions, each region can induce non-uniform deformation when a control signal is applied to the actuator. Consequently, it can induce non-uniform forces and moments when attached to plate or shell structures. The deformation function of each region of this new actuator system is defined next. With the deformation profile, the equivalent control forces and control moments are derived. Actuation and control characteristics of piezoelectric and photostrictive SQ actuator systems applied to plate and shell structures are respectively investigated later.

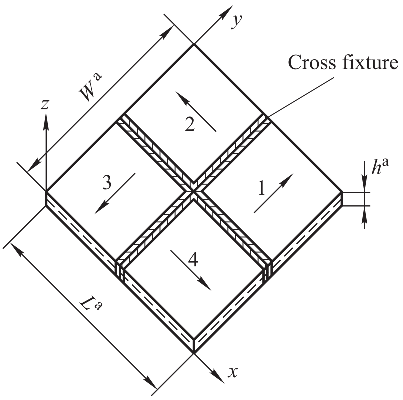

Fig. 1.3 A new SQ actuator system.

1.3 Plate control with a piezoelectric SQ actuator system

Piezoelectric SQ actuator design consists of four flexible mono-axial piezoelectric pieces or actuator regions. Based on the above calculations, distributions of induced non-uniform control forces and moments of each region are defined. Independent modal control actions of a square simply supported plate attached with the center-located and the corner-located SQ actuator are studied respectively in this section. In each case, control actions with different surface coverage (i.e., actuator sizes) are evaluated. Control effectiveness and modal actuations of these two locations are compared. Closed-loop control characteristics with four segmented sensors are used to regulate the sign of control voltages in each region and their control effectiveness is also evaluated in case studies.

1.3.1 Non-uniform forces and moments induced by the SQ actuator system

A new piezoelectric SQ actuator design consists of four flexible mono-axial piezoelectric elements respectively fixed to a center cross fixture. Figure 1.4 illustrates an SQ actuator system (with length L^{a} and width W^{a}) centrally placed on a plate (with length a and width b). When an electric control signal is applied to this actuator system, it induces non-uniform control forces and moments to the plate. The directions and distributions of induced control forces of each region are also shown in Fig.1.4. Non-uniform control forces and moments are defined in this section; modal control effects of rectangular plates are presented in the next section.

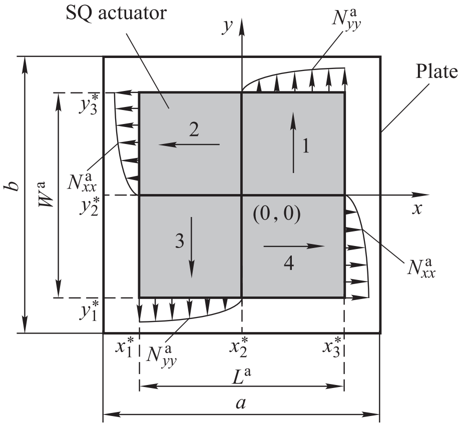

Fig. 1.4 A plate attached with a center-located SQ actuator system (not to scale).

According to the above variation procedures, the distribution profile of induced non-uniform forces and moments of each region can be written as

$$\begin{aligned} f_1(x) &= B_1 x b_1 + B_2 x^2 b_1 + B_3 x^2 b_1^2 + B_4 x b_1^2 + B_5 x^3 b_1^2 \\ &\quad + B_6 x^2 b_1^3 + B_7 x^3 b_1^3 + B_8 x^4 b_1^3 + B_9 x^3 b_1^4 + B_{10} x^4 b_1^4 \end{aligned} \tag{1.12}$$

$$\begin{aligned} f_2(y) &= -(B_1 y a_1 + B_2 y^2 a_1 + B_3 y^2 a_1^2 + B_4 y a_1^2 + B_5 y^3 a_1^2 \\ &\quad + B_6 y^2 a_1^3 + B_7 y^3 a_1^3 + B_8 y^4 a_1^3 + B_9 y^3 a_1^4 + B_{10} y^4 a_1^4) \end{aligned} \tag{1.13}$$

$$\begin{aligned} f_3(x) &= B_1 x b_1 - B_2 x^2 b_1 - B_3 x^2 b_1^2 + B_4 x b_1^2 + B_5 x^3 b_1^2 \\ &\quad - B_6 x^2 b_1^3 + B_7 x^3 b_1^3 - B_8 x^4 b_1^3 + B_9 x^3 b_1^4 - B_{10} x^4 b_1^4 \end{aligned} \tag{1.14}$$

$$\begin{aligned} f_4(y) &= -B_1 y a_1 + B_2 y^2 a_1 + B_3 y^2 a_1^2 - B_4 y a_1^2 - B_5 y^3 a_1^2 \\ &\quad + B_6 y^2 a_1^3 - B_7 y^3 a_1^3 + B_8 y^4 a_1^3 - B_9 y^3 a_1^4 + B_{10} y^4 a_1^4 \end{aligned} \tag{1.15}$$

Thus, the actuator induced control forces and moments (i.e., N_{ii}^{a} and M_{ii}^{a}) are

$$N_{xx}^{\mathrm{a}} = \frac{\bar{S}Y_{\mathrm{a}}}{L^{\mathrm{a}}/2} Y_{\mathrm{a}} h^{\mathrm{a}} \cdot \{f_4(y) \cdot [u_{\mathrm{s}}(x - x_2^*) - u_{\mathrm{s}}(x - x_3^*)] \cdot [u_{\mathrm{s}}(y - y_1^*) - u_{\mathrm{s}}(y - y_2^*)]$$
$$- f_2(y) \cdot [u_{\mathrm{s}}(x - x_1^*) - u_{\mathrm{s}}(x - x_2^*)] \cdot [u_{\mathrm{s}}(y - y_2^*) - u_{\mathrm{s}}(y - y_3^*)]\} \tag{1.16}$$

$$N_{yy}^{\mathrm{a}} = \frac{\bar{S}Y_{\mathrm{a}}}{W^{\mathrm{a}}/2} Y_{\mathrm{a}} h^{\mathrm{a}} \cdot \{f_1(x) \cdot [u_{\mathrm{s}}(x - x_2^*) - u_{\mathrm{s}}(x - x_3^*)] \cdot [u_{\mathrm{s}}(y - y_2^*) - u_{\mathrm{s}}(y - y_3^*)]$$
$$- f_3(x) \cdot [u_{\mathrm{s}}(x - x_1^*) - u_{\mathrm{s}}(x - x_2^*)] \cdot [u_{\mathrm{s}}(y - y_1^*) - u_{\mathrm{s}}(y - y_2^*)]\} \tag{1.17}$$

where $u_{\mathrm{s}}(\cdot)$ is a step function. The two sets of step functions define the location of the actuator induced forces. The actuator induced control moments are

$$M_{xx}^{\mathrm{a}} = N_{xx}^{\mathrm{a}} \cdot \frac{(h + h^{\mathrm{a}})}{2} \tag{1.18}$$

$$M_{yy}^{\mathrm{a}} = N_{yy}^{\mathrm{a}} \cdot \frac{(h + h^{\mathrm{a}})}{2} \tag{1.19}$$

Non-uniform control forces and moments induced by the new SQ actuator system are used to control the rectangular plate. Modal control effectiveness of plates is evaluated next.

1.3.2 Modal control

It is assumed that the transverse bending oscillation dominates the plate motion, i.e., the in-plane membrane oscillations are neglected. The transverse governing equation of the plate with the distributed actuator can be expressed as [21]

$$D\left(\frac{\partial^4 u_3}{\partial x^4} + 2\frac{\partial^4 u_3}{\partial x^2 \partial y^2} + \frac{\partial^4 u_3}{\partial y^4}\right) + \rho h \ddot{u}_3 + c\dot{u}_3 = \frac{\partial^2 M_{xx}^{\mathrm{a}}}{\partial x^2} + \frac{\partial^2 M_{yy}^{\mathrm{a}}}{\partial y^2} \tag{1.20}$$

where D is the bending stiffness, $D = Yh^3/(1 - \mu^2)$, Y is the plate Young's modulus, μ is the plate Poisson's ratio; ρ is the plate mass density; u_3 is the plate transverse displacement; h is the plate thickness; c is the damping constant; and $\ddot{u}_3$ and $\dot{u}_3$ are the plate transverse acceleration and velocity respectively. Note that the membrane control force does not contribute any control action to the transversely oscillating plate. It is also assumed that the plate is simply supported on all four edges. Based on the modal expansion technique, the dynamic response of the system can be represented by a sum of the responses of all participating modes, i.e.,

$$u_3(x,y,t) = \sum_{m=1}^{\infty} \sum_{n=1}^{\infty} \eta_{3mn}(t) U_{3mn}(x,y) \tag{1.21}$$

where U_{3mn} is the mn^{th} transverse mode shape function and η_{3mn} is the modal participation factor. Using the modal expansion and imposing the modal orthogonality of natural modes yields the mn^{th} transverse modal equation of the plate [21].

$$\ddot{\eta}_{mn} + 2\zeta_{mn}\omega_{mn}\dot{\eta}_{mn} + \omega_{mn}^2\eta_{mn} = F_{mn}^{\mathrm{c}} \tag{1.22}$$

where ζ_{mn} is the modal damping ratio, ω_{mn} is the natural frequency of the mn^{th} mode, and the modal control force F_{mn}^{c} is

$$F_{mn}^{\mathrm{c}} = \frac{1}{\rho h N_{mn}} \int_{-\frac{a}{2}}^{+\frac{a}{2}} \int_{-\frac{b}{2}}^{+\frac{b}{2}} \left(\frac{\partial^2 M_{xx}^{\mathrm{a}}}{\partial x^2} + \frac{\partial^2 M_{yy}^{\mathrm{a}}}{\partial y^2} \right) U_{3mn}(x,y)\mathrm{d}x\mathrm{d}y \tag{1.23}$$

where N_{mn} is defined by the squared mode shape functions:

$$N_{mn} = \int_x \int_y U_{3mn}^2 \mathrm{d}x\mathrm{d}y \tag{1.24}$$

In case studies, control actions and comparison of a center-located and a corner-located piezoelectric SQ actuator system on a square plate are respectively evaluated next.

1.3.3 Case studies: control of plates

As mentioned above, distributed modal actuations and control of a center-located and a corner-located piezoelectric SQ actuator system on a square plate are respectively investigated. Their modal actuation characteristics and effectiveness of these two cases are also compared.

1.3.3.1 Center-located piezoelectric SQ actuator on square plates

In this case, the SQ actuator is symmetrically located at the plate center and both the actuator and the plexiglas plate are square, that is $a = b$ and $L^{\mathrm{a}} = W^{\mathrm{a}}$. Dimensions of the square plate are 0.2 m × 0.2 m × 0.0016 m ($a \times b \times h$). Material properties of the plate and the actuator are listed in Appendix: Table 1.A1 and Table 1.A2. Since the structure and the actuator system are symmetrical, the origin is assumed at the center of the plate (Fig.1.4). Thus, the transverse mode shape function of a simply supported plate (with dimensions $a \times b$) in this coordinate system is

$$U_{3mn} = \sin\left[\frac{m\pi\left(x + \frac{a}{2}\right)}{a}\right] \cdot \sin\left[\frac{n\pi\left(y + \frac{b}{2}\right)}{b}\right] \tag{1.25}$$

where a and b are respectively the length and the width of the plate. Effects of actuator sizes defined by the length ratio Δ, i.e., $\Delta = L^{\mathrm{a}}/a$ (actuator length/plate length), are also evaluated. Substituting Eqs.(1.18), (1.24) and (1.25) into the first term of the right side of the modal control force in Eq.(1.23) yields

$$
\begin{aligned}
&\frac{4}{\rho hab}\int_{-\frac{a}{2}}^{+\frac{a}{2}}\int_{-\frac{b}{2}}^{+\frac{b}{2}}\left(\frac{\partial^2 M_{xx}^{\mathrm{a}}}{\partial x^2}\right)U_{3mn}(x,y)\mathrm{d}x\mathrm{d}y\\
&=\frac{4}{\rho hab}\frac{\overline{S}Y_{\mathrm{a}}}{\frac{L^{\mathrm{a}}}{2}}Y_{\mathrm{a}}h^{\mathrm{a}}\frac{(h+h^{\mathrm{a}})}{2}\int_{-\frac{a}{2}}^{+\frac{a}{2}}\int_{-\frac{b}{2}}^{+\frac{b}{2}}\frac{\partial^2}{\partial x^2}\{f_4(y)\cdot[u_{\mathrm{s}}(x-x_2^*)\\
&\quad -u_{\mathrm{s}}(x-x_3^*)]\cdot[u_{\mathrm{s}}(y-y_1^*)-u_{\mathrm{s}}(y-y_2^*)]\\
&\quad -f_2(y)\cdot[u_{\mathrm{s}}(x-x_1^*)-u_{\mathrm{s}}(x-x_2^*)]\cdot[u_{\mathrm{s}}(y-y_2^*)-u_{\mathrm{s}}(y-y_3^*)]\}U_{3mn}(x,y)\mathrm{d}x\mathrm{d}y\\
&=\overline{S}\tilde{M}_{xmn}
\end{aligned}
\tag{1.26}
$$

Similarly, substituting Eqs.(1.18), (1.19), (1.24) and (1.25) into the second term of the modal control force in Eq.(1.23) gives

$$
\begin{aligned}
&\frac{4}{\rho hab}\int_{-\frac{a}{2}}^{+\frac{a}{2}}\int_{-\frac{b}{2}}^{+\frac{b}{2}}\left(\frac{\partial^2 M_{yy}^{\mathrm{a}}}{\partial y^2}\right)U_{3mn}(x,y)\mathrm{d}x\mathrm{d}y\\
&=\frac{4}{\rho hab}\frac{\overline{S}Y_{\mathrm{a}}}{\frac{W^{\mathrm{a}}}{2}}Y_{\mathrm{a}}h^{\mathrm{a}}\frac{(h+h^{\mathrm{a}})}{2}\int_{-\frac{a}{2}}^{+\frac{a}{2}}\int_{-\frac{b}{2}}^{+\frac{b}{2}}\frac{\partial^2}{\partial y^2}\{f_1(x)\cdot[u_{\mathrm{s}}(x-x_2^*)\\
&\quad -u_{\mathrm{s}}(x-x_3^*)]\cdot[u_{\mathrm{s}}(y-y_2^*)-u_{\mathrm{s}}(y-y_3^*)]\\
&\quad -f_3(x)\cdot[u_{\mathrm{s}}(x-x_1^*)-u_{\mathrm{s}}(x-x_2^*)]\cdot[u_{\mathrm{s}}(y-y_1^*)-u_{\mathrm{s}}(y-y_2^*)]\}U_{3mn}(x,y)\mathrm{d}x\mathrm{d}y\\
&=\overline{S}\tilde{M}_{ymn}
\end{aligned}
\tag{1.27}
$$

The actuator is located from coordinates x_1^* to x_3^* and y_1^* to y_3^*. As shown in Fig.1.4, $x_1^*=-L^{\mathrm{a}}/2$, $x_2^*=0$, $x_3^*=L^{\mathrm{a}}/2$, $y_1^*=-W^{\mathrm{a}}/2$, $y_2^*=0$, and $y_3^*=+W^{\mathrm{a}}/2$. Substituting Eqs.(1.26) and (1.27) into Eq.(1.23), one obtains

$$
F_{mn}^{\mathrm{c}}=\overline{S}\cdot(\tilde{M}_{xmn}+\tilde{M}_{ymn})=\overline{S}\cdot\tilde{F}_{mn}^{\mathrm{c}}
\tag{1.28}
$$

Thus, the total control action $\tilde{F}_{mn}^{\mathrm{c}}$ (i.e., the magnitude of control moments) becomes

$$
\tilde{F}_{mn}^{\mathrm{c}}=\tilde{M}_{xmn}+\tilde{M}_{ymn}
\tag{1.29}
$$

where control actions $\tilde{M}_{xmn}$ and $\tilde{M}_{ymn}$ denote "actuation magnitudes" which are used as comparison indices in future comparisons. Note that for an unbiased comparison, the magnitude and sign of control voltages applied to the actuator system remains unchanged in all cases. The modal control effectiveness of the actuator can be evaluated with these control actions. Recall that the control action is determined by the material properties, actuator and plate dimensions, the mode number and the location of the actuator. Modal control actions of the new SQ actuator with different length ratios (Δ = 1/4, 1/3, 1/2, 2/3, 3/4, 1) or actuator coverage are calculated and summarized in Table 1.2.

This table suggests that the new SQ actuator has control effects on square plates only when both m and n are odd wave numbers. Because the location of the actuator is center-located and the mode shape function of the simply supported plate, the symmetrical

Table 1.2 Control actions of the center-located SQ actuator. (unit: N/kg)

Mode \ Δ	1/4	1/3	1/2	2/3	3/4	1
(1,1)	–1397	–2370	–4646	–6752	–7520	–7963
(1,2)	0	0	0	0	0	0
(1,3)	5580	7773	7230	–1173	–6720	–15345
(2,1)	0	0	0	0	0	0
(2,2)	0	0	0	0	0	0
(2,3)	0	0	0	0	0	0
(3,1)	5580	7773	7230	–1173	–6720	–15345
(3,2)	0	0	0	0	0	0
(3,3)	–7520	–7963	–1566	0	–5090	–20403

modes, such as (1,1), (1,3), (3,3), etc., are effectively controlled. But the anti-symmetrical modes, such as (2,2), (2,4), etc., are not controllable, because the positive and negative control actions cancel out each other. To further evaluate the SQ actuator, plot this actuators' control actions of the square plate with respect to the actuator/plate length ratio ($\Delta = L^a/L$) in Fig.1.5. Because it has no control effects on even modes when $m = 2$, e.g., (2,1), (2,2), (2,3), only the control actions of odd mode groups of $m = 1$ (Fig.1.5(a)) and $m = 3$ (Fig.1.5(b)), e.g., (1,1), (1,2), (1,3), (3,1), (3,2), and (3,3), are plotted.

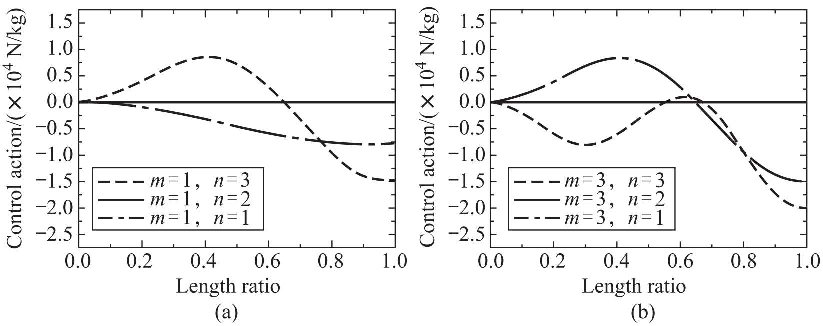

Fig. 1.5 Control actions of the center-located SQ actuator. (a) (1,1), (1,2), (1,3) modes; (b) (3,1), (3,2), (3,3) modes.

From these two figures, it can be observed that the actuator has identical control actions on modes (1,3) and (3,1), due to symmetry. The control actions on all controllable modes fluctuate with respect to the length ratio, i.e., the actuator coverage. Thus, the actuator size is very important to the overall modal control effectiveness. Figure 1.5(b) shows that the new SQ actuator performs best on mode (3,3) when the length ratio approaches to 1. This is contributed by the actuator configurations and the mode shape function of simply supported plates. Note that the (3,3) actuation magnitude of the SQ actuator is much larger (about 48%) than that of the multi-DOF actuator [34], due to its non-uniform boundary conditions, when $\Delta = 1$. As shown in Fig.1.6, the plate nodal lines of mode (3,3) and the actuator area are respectively drawn in dashed lines and solid lines, and the mode shapes are represented by "+" and "–" regions. Because in this case the sign and magnitude of control voltage do not change, the real control action of mode (3,3) is the difference between the control actions of "+" and "–" regions. Since the new SQ

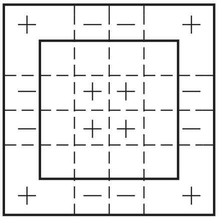

Fig. 1.6 Control effectiveness of mode (3,3).

actuator induces non-uniform control forces and moments, it performs better at its four corners. When the length ratio approaches to 1, the induced control actions on the "+" regions would be much more significant than those on the "–" regions.

Thus, this center-located SQ actuator is only effective to odd modes and ineffective to even modes. Accordingly, control effectiveness of a corner-located SQ actuator system is evaluated next.

1.3.3.2 Corner-located piezoelectric SQ actuator on square plates

In this case, the SQ actuator is located at one quadrant of the square plate. The dimensional and material properties of the square plate and those of the actuator are the same as before. In order to simplify the calculation, the origin of the coordinate system is assumed at the center of the actuator, as shown in Fig.1.7.

Following the previous procedures, one can define the modal control force of the corner-located actuator system.

$$F_{mn}^{\mathrm{c}} = \frac{1}{\rho h N_{mn}} \int_{-\frac{a}{4}}^{+\frac{3a}{4}} \int_{-\frac{b}{4}}^{+\frac{3b}{4}} \left(\frac{\partial^2 M_{xx}^{\mathrm{a}}}{\partial x^2} + \frac{\partial^2 M_{yy}^{\mathrm{a}}}{\partial y^2} \right) U_{3mn}(x,y)\mathrm{d}x\mathrm{d}y \tag{1.30}$$

where the modal shape function in this new coordinate system can be rewritten as

$$U_{3mn} = \sin\left[\frac{m\pi\left(x+\frac{a}{4}\right)}{a}\right] \sin\left[\frac{n\pi\left(y+\frac{b}{4}\right)}{b}\right] \tag{1.31}$$

and

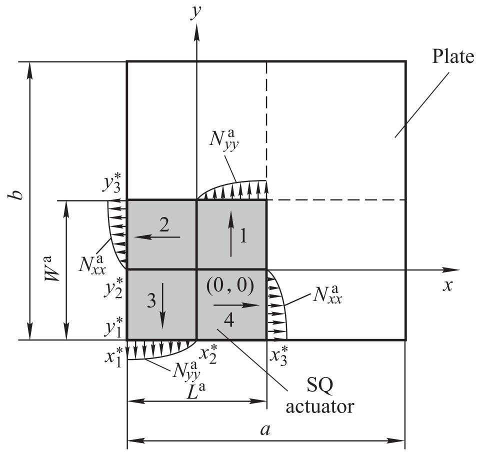

Fig. 1.7 The SQ actuator system is located at one corner of the plate.

$$N_{mn} = \int_x \int_y U_{3mn}^2 \mathrm{d}x\mathrm{d}y = \int_{-\frac{a}{4}}^{+\frac{3a}{4}} \int_{-\frac{b}{4}}^{+\frac{3b}{4}} \sin^2\left[\frac{m\pi\left(x+\frac{a}{4}\right)}{a}\right] \sin^2\left[\frac{n\pi\left(y+\frac{b}{4}\right)}{b}\right] \mathrm{d}x\mathrm{d}y = \frac{ab}{4} \tag{1.32}$$

Substituting Eqs.(1.31) and (1.32) into Eq.(1.30) yields the two control moments induced by the corner-placed actuator system:

$$\begin{aligned}
&\frac{4}{\rho hab}\int_{-\frac{a}{4}}^{+\frac{3a}{4}}\int_{-\frac{b}{4}}^{+\frac{3b}{4}}\left(\frac{\partial^2 M_{xx}^{\mathrm{a}}}{\partial x^2}\right)U_{3mn}(x,y)\mathrm{d}x\mathrm{d}y\\
&= \frac{4}{\rho hab}\frac{\overline{S}Y_{\mathrm{a}}}{\frac{1}{2}L^{\mathrm{a}}}Y_{\mathrm{a}}h^{\mathrm{a}}\frac{(h+h^{\mathrm{a}})}{2}\int_{-\frac{a}{4}}^{+\frac{3a}{4}}\int_{-\frac{b}{4}}^{+\frac{3b}{4}}\frac{\partial^2}{\partial x^2}\{f_4(y)\cdot[u_{\mathrm{s}}(x-x_2^*)-u_{\mathrm{s}}(x-x_3^*)]\\
&\quad\cdot[u_{\mathrm{s}}(y-y_1^*)-u_{\mathrm{s}}(y-y_2^*)]-f_2(y)\cdot[u_{\mathrm{s}}(x-x_1^*)-u_{\mathrm{s}}(x-x_2^*)]\\
&\quad\cdot[u_{\mathrm{s}}(y-y_2^*)-u_{\mathrm{s}}(y-y_3^*)]\}U_{3mn}(x,y)\mathrm{d}x\mathrm{d}y\\
&= \overline{S}\tilde{M}_{xmn}
\end{aligned} \tag{1.33}$$

$$\begin{aligned}
&\frac{4}{\rho hab}\int_{-\frac{a}{4}}^{+\frac{3a}{4}}\int_{-\frac{b}{4}}^{+\frac{3b}{4}}\left(\frac{\partial^2 M_{yy}^{\mathrm{a}}}{\partial y^2}\right)U_{3mn}(x,y)\mathrm{d}x\mathrm{d}y\\
&= \frac{4}{\rho hab}\frac{\overline{S}Y_{\mathrm{a}}}{\frac{1}{2}W^{\mathrm{a}}}Y_{\mathrm{a}}h^{\mathrm{a}}\frac{(h+h^{\mathrm{a}})}{2}\int_{-\frac{a}{4}}^{+\frac{3a}{4}}\int_{-\frac{b}{4}}^{+\frac{3b}{4}}\frac{\partial^2}{\partial y^2}\{f_1(x)\cdot[u_{\mathrm{s}}(x-x_2^*)-u_{\mathrm{s}}(x-x_3^*)]\\
&\quad\cdot[u_{\mathrm{s}}(y-y_2^*)-u_{\mathrm{s}}(y-y_3^*)]-f_3(x)\cdot[u_{\mathrm{s}}(x-x_1^*)-u_{\mathrm{s}}(x-x_2^*)]\\
&\quad\cdot[u_{\mathrm{s}}(y-y_1^*)-u_{\mathrm{s}}(y-y_2^*)]\}U_{3mn}(x,y)\mathrm{d}x\mathrm{d}y\\
&= \overline{S}\tilde{M}_{ymn}
\end{aligned} \tag{1.34}$$

Similarly, the total control action $\tilde{F}^{c}_{mn}$ (i.e., the magnitude of control moments) becomes

$$\tilde{F}^{c}_{mn} = \tilde{M}_{xmn} + \tilde{M}_{ymn} \tag{1.35}$$

Assume the length ratio is set as its maximal value, i.e., $\Delta = 1/2$, comparisons of mode control actions between the center-located actuator and the corner-located actuator are summarized in Table 1.3. This table indicates that the corner-located actuator leads to control effectiveness on all of the first nine modes. It provides the same control actions on modes (1,2) and (2,1), (2,3) and (3,2), and less control actions on modes (1,1), (1,3) and (3,3), as compared with the center-located actuator when the length ratio is 1/2.

Table 1.3 Comparison of mode control actions ($\Delta = 1/2$). (unit: N/kg)

Mode	Corner-located	Center-located
(1,1)	–2323	–4646
(1,2)	–5641	0
(1,3)	314	7230
(2,1)	–5641	0
(2,2)	–7963	0
(2,3)	–3509	0
(3,1)	–7544	7230
(3,2)	–3509	0
(3,3)	–784	–1566

Magnitudes of control actions on all controllable modes also fluctuate with respect to the length ratio or actuator size, as shown in Figs.1.8(a)-(c). These figures indicate that when the length ratio is $\Delta = 1/2$, the actuator introduce the maximal control action on modes (1,1), (1,2), (2,1), and (3,1). However, it does not provide the best control action on modes (1,3), (2,2), (2,3), (3,2), (3,3). Unlike the center-located actuator, the maximal coverage size of corner-located actuator is only 1/4, i.e., $\Delta = 1/2$.

The comparison between Fig.1.8 and Fig.1.5 suggests that the center-located actuator performs better on symmetrical modes, such as (1,1), (1,3), (3,3), etc. The corner-located actuator improves the control actions on anti-symmetrical modes, but degrades the control effects on symmetrical modes. Another method to improve the modal control effectiveness of the center-located SQ actuator is discussed next.

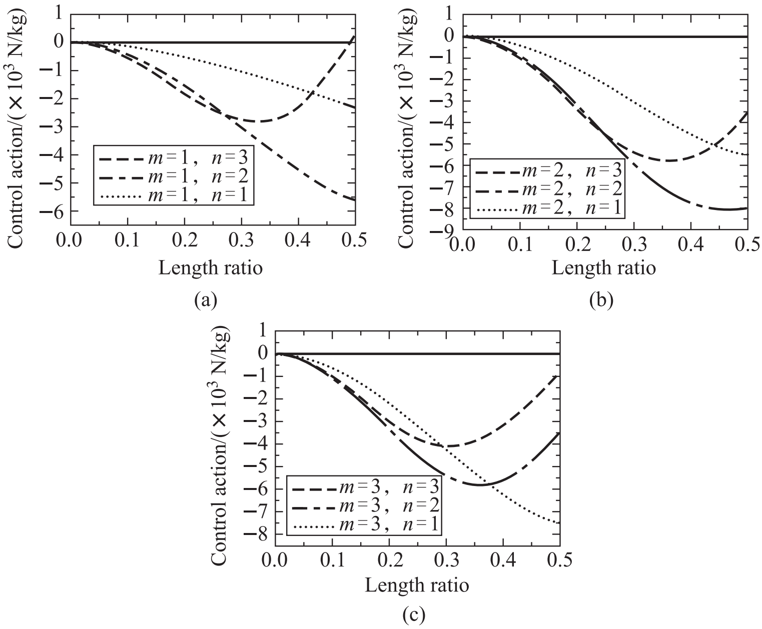

Fig. 1.8 Modal control actions and size relationship of the corner-located SQ actuator system. (a) (1,1), (1,2), (1,3) modes; (b) (2,1), (2,2), (2,3) modes; (c) (3,1), (3,2), (3,3) modes.

1.3.4 Closed-loop actuation with collocated sensors and actuators

As discussed previously, the corner-located actuator can control more modes than the center-located actuator. However, it is less effective than the center-located actuator in symmetrical plate modes, such as the (1,1) mode. To improve the control effectiveness, the sensor segmentation technique and closed-loop feedback [21] are used to enable the center-located SQ actuator to control all of the first nine modes. As shown in Fig.1.9,

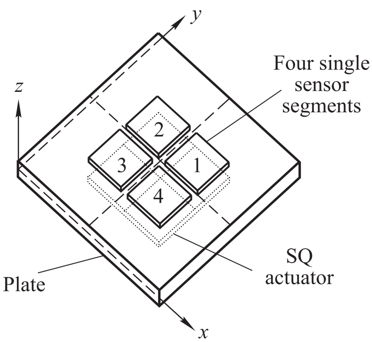

Fig. 1.9 A plate attached with four sensor segments and a center-located SQ actuator system.

four segmented biaxial piezoelectric sensors are located symmetrically to the plate's center. Each sensor segment responds to the local motion state and generates a signal output which is fed back to its collocated region of the SQ actuator. In order to prevent the sensors from short-circuiting, it is assumed that a small gap is left open between the two adjacent sensor segments, but it is ignored in the mathematical model due to its smallness.

Because the sensing signals are primarily contributed by bending strains of the plate in the transverse oscillation, membrane strains due to in-plane oscillation are ignored. The mn^{th} unit modal sensing signal of distributed piezoelectric sensor ϕ^{s}_{mn} can be expressed as a function of mode shape functions [13]:

$$\phi^{\text{s}}_{mn} = -h^{\text{s}}\left[h_{31}r^{\text{s}}_1\left(\frac{\partial^2 U_{3mn}}{\partial x^2}\right) + h_{32}r^{\text{s}}_2\left(\frac{\partial^2 U_{3mn}}{\partial y^2}\right)\right] \tag{1.36a}$$

$$\phi^{\text{s}}_{mn} = -(h^{\text{s}}/A^{\text{s}})\int_{A^{\text{s}}}\left[h_{31}r^{\text{s}}_1\left(\frac{\partial^2 U_{3mn}}{\partial x^2}\right) + h_{32}r^{\text{s}}_2\left(\frac{\partial^2 U_{3mn}}{\partial y^2}\right)\right]\mathrm{d}A^{\text{s}} \tag{1.36b}$$

where h^{s} is the thickness of the distributed piezoelectric sensor layer, A^{s} is the effective electrode sensor area, h_{31} and h_{32} are piezoelectric constants, r^{s}_i denotes the distance measured from the neutral surface to the mid-plane of the sensor layer, and $r^{\text{s}}_i = (h + h^{\text{s}}_i)/2$. Note that $r^{\text{s}}_1 = r^{\text{s}}_2 = (h + h^{\text{s}})/2$ for uniform-thickness plates and sensor segments. Equation (1.36a) denotes the spatial distribution and Eq.(1.36b) denotes the averaged signal output of the sensor segment. It is assumed that four distributed piezoelectric sensors cover the whole surface of the plate. In order to simplify the calculation, the origin of the coordinate system is set at the center of the plate. For the mn^{th} mode, the output signals ϕ^{s}_{mn} of four sensor segments are respectively [12]

$$\begin{aligned}
\phi^{\text{s1}}_{mn} &= (h^{\text{s}}/A^{\text{s1}})[h_{31}r^{\text{s}}_1(m\pi/a)^2 + h_{32}r^{\text{s}}_2(n\pi/b)^2] \\
&\quad\times \int_0^{a/2}\int_0^{b/2} \sin[m\pi(x+a/2)/a]\sin[n\pi(y+b/2)/b]\mathrm{d}x\mathrm{d}y \\
&= 4S_{mn}[\cos(m\pi/2) - \cos(m\pi)]\cdot[\cos(n\pi/2) - \cos n\pi] && (1.37) \\
\phi^{\text{s2}}_{mn} &= 4S_{mn}[1 - \cos(m\pi/2)]\cdot[\cos(n\pi/2) - \cos n\pi] && (1.38) \\
\phi^{\text{s3}}_{mn} &= 4S_{mn}[1 - \cos(m\pi/2)]\cdot[1 - \cos(n\pi/2)] && (1.39) \\
\phi^{\text{s4}}_{mn} &= 4S_{mn}[\cos(m\pi/2) - \cos m\pi][1 - \cos(n\pi/2)] && (1.40)
\end{aligned}$$

where $S_{mn} = (h^{\text{s}}/mn)[h_{31}r^{\text{s}}_1(m/a)^2 + h_{32}r^{\text{s}}_2(n/b)^2]$ is the mn^{th} modal sensitivity. With the above four signal equations, the output signals exist for most modes, except for either m or n is multiples of 4. The sign of feedback voltages to each region of the SQ actuator is regulated for different plate modes, and $\phi^{\text{s1}}_{mn} = (-1)^m\cdot(-1)^n\phi^{\text{s3}}_{mn}$, $\phi^{\text{s2}}_{mn} = (-1)\cdot(-1)^n\phi^{\text{s3}}_{mn}$, $\phi^{\text{s4}}_{mn} = (-1)\cdot(-1)^m\phi^{\text{s3}}_{mn}$. Again, it is assumed that the amplitude of feedback voltage of each sensor is kept at a constant maximum $|\phi^{\text{a}}|$, and only the sign of each sensor's voltage is regulated with respect to the wave number, i.e., $\phi^{\text{s1}}_{mn} = (-1)^m\cdot(-1)^n|\phi^{\text{a}}|$, $\phi^{\text{s2}}_{mn} = (-1)\cdot(-1)^n|\phi^{\text{a}}|$, $\phi^{\text{s3}}_{mn} = |\phi^{\text{a}}|$, $\phi^{\text{s4}}_{mn} = (-1)\cdot(-1)^m|\phi^{\text{a}}|$, for both m and n are odd number modes, such as modes (1,1), (1,3), (3,1), (3,3). Thus, this SQ actuator would induce identical control actions as that without four sensors. However, for either m or n is even mode, such as (1,2), (2,1), (2,2), (2,3), (3,2), regulating the sign of feedback voltages can introduce control effects to even modes and this is different from the earlier case with a single uniform control voltage. When this SQ actuator is laminated with a plate, the desired induced control forces/moments on even modes of its four regions are illustrated in Fig.1.10.

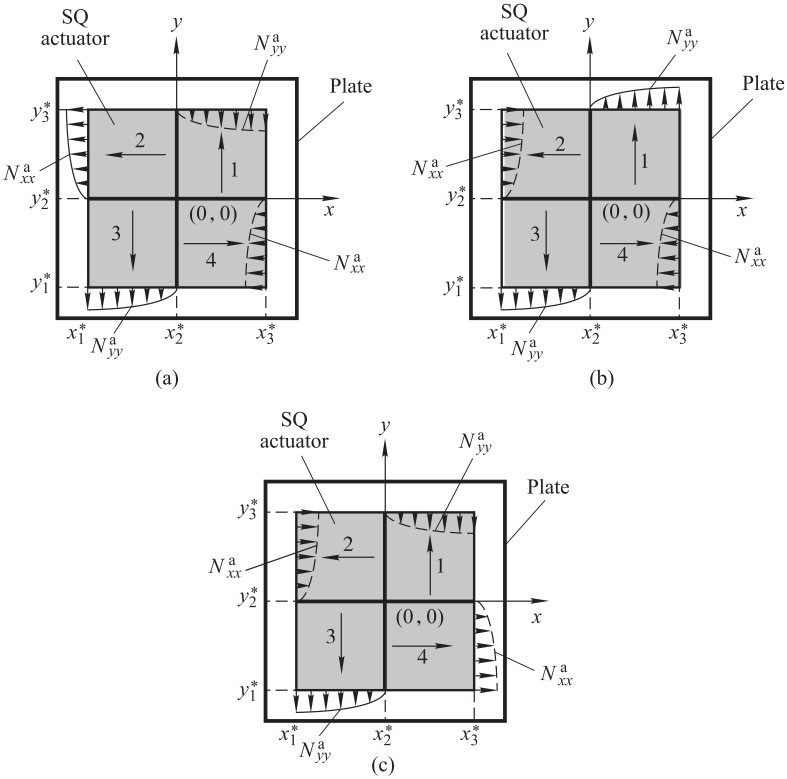

Fig. 1.10 A plate attached with a center-located SQ actuator system and collocated sensor segments. (a) (2,1), (2,3) modes; (b) (2,2) mode; (c) (3,2) mode.

Based on these signal output, the actuator induced modal control actions are

$$\frac{4}{\rho hab}\int_{-\frac{a}{2}}^{+\frac{a}{2}}\int_{-\frac{b}{2}}^{+\frac{b}{2}}\left(\frac{\partial^2 M_{xx}^{\mathrm{a}}}{\partial x^2}\right)U_{3mn}(x,y)\mathrm{d}x\mathrm{d}y$$

$$=\frac{4}{\rho hab}\frac{\bar{S}Y_{\mathrm{a}}}{\frac{1}{2}L^{\mathrm{a}}}Y_{\mathrm{a}}h^{\mathrm{a}}\frac{(h+h^{\mathrm{a}})}{2}$$

$$\times\int_{-\frac{a}{2}}^{+\frac{a}{2}}\int_{-\frac{b}{2}}^{+\frac{b}{2}}\frac{\partial^2}{\partial x^2}\{-(-1)^m\cdot f_4(y)\cdot[u_{\mathrm{s}}(x-x_2^*)-u_{\mathrm{s}}(x-x_3^*)]$$

$$
\begin{aligned}
&\cdot[u_s(y-y_1^*)-u_s(y-y_2^*)]+(-1)^n\cdot f_2(y)\cdot[u_s(x-x_1^*)-u_s(x-x_2^*)]\\
&\cdot[u_s(y-y_2^*)-u_s(y-y_3^*)]\}U_{3mn}(x,y)\mathrm{d}x\mathrm{d}y\\
=\,&\overline{S}\tilde{M}_{xmn}
\end{aligned}
\tag{1.41}
$$

$$
\begin{aligned}
&\frac{4}{\rho hab}\int_{-\frac{a}{2}}^{+\frac{a}{2}}\int_{-\frac{b}{2}}^{+\frac{b}{2}}\left(\frac{\partial^2 M_{yy}^{\mathrm{a}}}{\partial y^2}\right)U_{3mn}(x,y)\mathrm{d}x\mathrm{d}y\\
=\,&\frac{4}{\rho hab}\frac{\overline{S}Y_{\mathrm{a}}}{\frac{1}{2}W^{\mathrm{a}}}Y_{\mathrm{a}}h^{\mathrm{a}}\frac{(h+h^{\mathrm{a}})}{2}\\
&\times\int_{-\frac{a}{2}}^{+\frac{a}{2}}\int_{-\frac{b}{2}}^{+\frac{b}{2}}\frac{\partial^2}{\partial y^2}\{(-1)^m\cdot(-1)^n\cdot f_1(x)\cdot[u_s(x-x_2^*)-u_s(x-x_3^*)]\\
&\cdot[u_s(y-y_2^*)-u_s(y-y_3^*)]-f_3(x)\cdot[u_s(x-x_1^*)-u_s(x-x_2^*)]\\
&\cdot[u_s(y-y_1^*)-u_s(y-y_2^*)]\}U_{3mn}(x,y)\mathrm{d}x\mathrm{d}y\\
=\,&\overline{S}\tilde{M}_{ymn}
\end{aligned}
\tag{1.42}
$$

where

$$
\overline{S}=(d_{31}\cdot|\phi^{\mathrm{a}}|)/h^{\mathrm{a}}
\tag{1.43}
$$

Closed-loop control actions of the new SQ actuator with different length ratios ($\varDelta$ = 1/4, 1/3, 1/2, 2/3, 3/4, 1) are summarized in Table 1.4.

Table 1.4 Control actions of the center-located SQ actuator. (unit: N/kg)

$\varDelta$ / Mode	1/4	1/3	1/2	2/3	3/4	1
(1,1)	–1397	–2370	–4646	–6752	–7520	–7963
(1,2)	–1397	–3098	–8599	–15333	–18239	–20982
(1,3)	5580	7773	7230	–1173	–6720	–15345
(2,1)	–1397	–3098	–8599	–15333	–18239	–20982
(2,2)	–1004	–2912	–11477	–25213	–32108	–40448
(2,3)	3169	5695	6826	–4062	–12966	–28770
(3,1)	5580	7773	7230	–1172	–6720	–15345
(3,2)	3169	5695	6826	–4062	–12966	–28770
(3,3)	–7520	–7963	–1566	0	–5090	–20403

Table 1.4 suggests that the actuator induces identical actuation magnitudes on modes (1,2) and (2,1), (1,3) and (3,1), (2,3) and (3,2). Comparing Table 1.2 with Table 1.4 suggests that when both n and m are odd numbers, such as (1,1), (1,3), (3,1), (3,3) mode, either with or without segmented sensors, the control actions of the SQ actuator system are identical. Thus, with the collocated sensors, the control actions for even modes can be improved without degrading the control actions for odd modes. The control actions and the size relationship of the first nine modes are plotted in Fig.1.11 to further illustrate